J Mater Sci (2009) 44:2610–2616
DOI 10.1007/s10853-009-3341-y

Filament poisoning at typical carbon nanotube deposition conditions by hot-filament CVD

C. J. Oliphant · C. J. Arendse · G. F. Malgas · D. E. Motaung · T. F. G. Muller · S. Halindintwali · B. A. Julies · D. Knoesen

Received: 3 December 2008 / Accepted: 11 February 2009 / Published online: 6 March 2009

Abstract We report on the poisoning of tungsten filaments during the hot-filament chemical vapour deposition process at typical carbon nanotube (CNT) deposition conditions and filament temperatures ranging from 1400 to 2000 °C. The morphological and structural changes of the filaments were investigated using scanning electron microscopy and X-ray diffraction, respectively. Our results conclusively show that the W-filament is not stable during the carburization process and that both mono- and ditungsten-carbides form within the first 5 min. Cracks and graphitic microspheres form on the carbide layer during the first 15 min at the temperatures ≥1600 °C. The microspheres subsequently coalesce to form a graphite layer, encapsulating a fully carburized filament at the temperature of 2000 °C after 60 min, which inhibits the catalytic activity of the filament to produce atomic hydrogen. The structural changes of the filament also induce variations in its temperature, illustrating the instability of the filament during the deposition of CNTs.

C. J. Oliphant · C. J. Arendse (✉) · D. E. Motaung · T. F. G. Muller · S. Halindintwali · B. A. Julies · D. Knoesen
Department of Physics, University of the Western Cape, Private Bag X17, Bellville 7535, South Africa
e-mail: cjarendse@uwc.ac.za

C. J. Oliphant · C. J. Arendse · G. F. Malgas (✉) · D. E. Motaung
National Centre for Nano-Structured Materials, CSIR Materials Science and Manufacturing, P.O. Box 395, Pretoria 0001, South Africa
e-mail: gmalgas@csir.co.za

Introduction

The hot-filament chemical vapour deposition (HFCVD) process has been extensively used for the deposition of various materials, including diamond [1–4], polymers [5], silicon thin films [6], boron–carbon–nitride layers [7], tungsten oxide nanoparticles [8] and carbon nanotubes (CNTs) [9]. The process relies on the catalytic decomposition of precursor gases into reactive gaseous species by a resistively heated filament. A variety of transition metals, such as tungsten (W), tantalum (Ta) and rhenium (Re), have been utilized as the filament during the HFCVD process [10–12]. This is primarily due to their high melting points and superior mechanical stabilities at temperatures above 1500 °C. Furthermore, different filaments have different abilities to dissociate the precursors. For example, a Ta filament dissociates molecular hydrogen (H_2) into atomic hydrogen (H^0) twice as efficient as a W filament during the deposition of microcrystalline silicon thin films [10].

Reactions between the precursor gases and the heated filament result in changes of the structural properties of the filaments; a process referred to as filament ageing. The most comprehensive study on the filament ageing process in a methane atmosphere, hereafter referred to as filament carburization, was executed for the synthesis of diamond [1, 11, 13–18]. Filament carburization has several implications for HFCVD; of which the most notable is that the catalytic ability of the filament changes during carburization, since the structure and the temperature of the filament vary during the deposition [10], which consequently results in unstable deposition conditions. Furthermore, from a manufacturing point of view, carbides are brittle materials and therefore the formation thereof reduces the lifetime of the filament.

The structure and properties of CNTs deposited by HFCVD are a direct consequence of the deposition parameters, such as the growth temperature, deposition pressure, gas mixtures and flow rates. These effects are usually reported in the literature [9, 19, 20], with the assumption that the structure and temperature of the filament remain stable during deposition. We therefore report on the stability of the morphology, structure and temperature of the W-filament at typical CNT deposition conditions [9, 19, 20], probed as a function of exposure time and filament temperature, using scanning electron microscopy (SEM), X-ray diffraction (XRD) and in situ temperature measurements, respectively. Furthermore, the morphology of the resultant CNTs will be compared and related to the structural changes of the filament for different filament temperatures.

Experimental

The filaments

Coiled W-filaments (99.95% purity) of length 350 mm and diameter 0.5 mm were carburized in a quartz tube HFCVD reactor [20], using a CH_4:H_2 atmosphere of 1:10 at a deposition pressure of 150 Torr. The filaments were resistively heated to its desired temperature by a 1-kW DC power supply and its temperature was measured using a two-colour optical pyrometer (Raytek® Marathon MR1S series, 0.75% error), located ~1.5-m away from the filament. Exposure times amounted to 5, 15 and 60 min at temperatures ranging from 1400 to 2000 °C, with a step size of 200 °C. The temperature of the filament was monitored in situ as a function of time during carburization with a resolution of 1 min. After carburization, the filaments were allowed to cool down to room temperature in vacuum, later they were removed and then stored away for analysis. The filaments were highly brittle after the carburization and therefore great care was taken when removing the filaments in order to prevent any mechanical disturbance to its surface.

Characterization

Cross sections of the carburized filaments were prepared by grinding and subsequent polishing using diamond lapping films. The surface and cross sections of the W-filaments were examined using a Hitachi X-650 SEM operated at 12–25 kV. Elemental composition of the filament was performed at an accelerating voltage of 12 kV, using the EDAX® system for energy dispersive spectroscopy (EDS) with a detector resolution of 140 eV. The morphology of the CNTs was characterized using a LEO 1525 field emission scanning electron microscope operated at 3–10 kV. Phase identification, performed on a coil from the central part of the filament, was measured using the Phillips PW 1830 X-ray powder diffractometer in a θ–2θ geometry, operated at 45 kV and 40 mA. The XRD spectra were collected at 2θ-values ranging from 10 to 80° with a step size of 0.02°. Copper $K\alpha_1$ radiation with a wavelength of 1.5406 Å was used as the X-ray source. The tungsten, tungsten-carbide and graphite phases were identified using the diffraction pattern database maintained by the International Centre for Diffraction Data (ICDD) [21].

Results and discussion

Figure 1 shows an SEM micrograph of an industrially pure W-filament and its XRD spectrum (inset) as reference. Three characteristic XRD peaks are evident which are associated with the tungsten body centred cubic crystal structure. The surface of the filament has grooves, indicating that it was produced by an extrusion method. Furthermore, the surface is covered with carbonaceous impurities which confirm the need to heat the filament prior to deposition in order to remove any impurities from its surface.

The SEM micrographs of the centre sections of filaments operated at 1400 °C for 5 and 15 min are depicted in Fig. 2. The filament shows minimal morphological changes. However, XRD reveals that the filament surface has carburized to ditungsten carbide (W_2C) and monotungsten carbide (WC) during the first 5 min (Fig. 3). Subsequently, the WC phase dominates after 15 min, as suggested by the increase in its XRD intensities relative to the W_2C and the

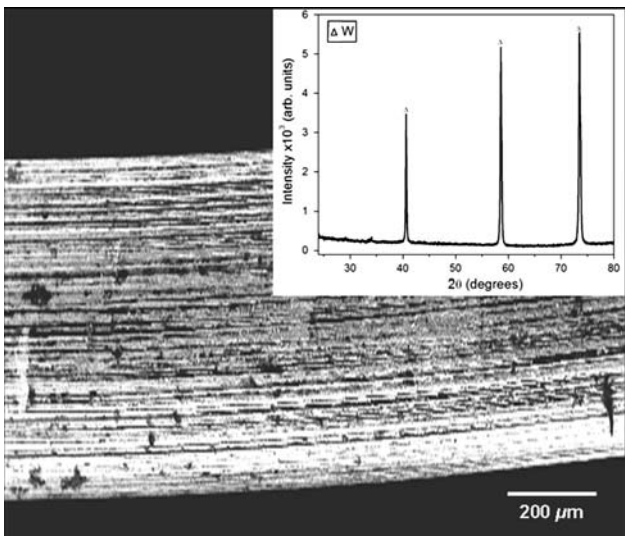

Fig. 1 Secondary electron SEM micrograph of an industrially pure W-filament and its XRD spectrum (inset)

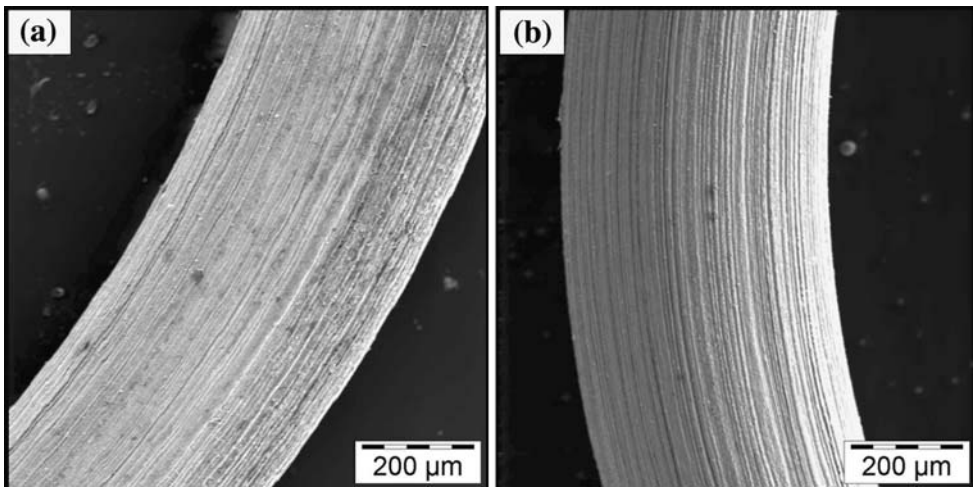

Fig. 2 Secondary electron SEM micrographs of the filament–surface operated at 1400 °C for **a** 5 min and **b** 15 min

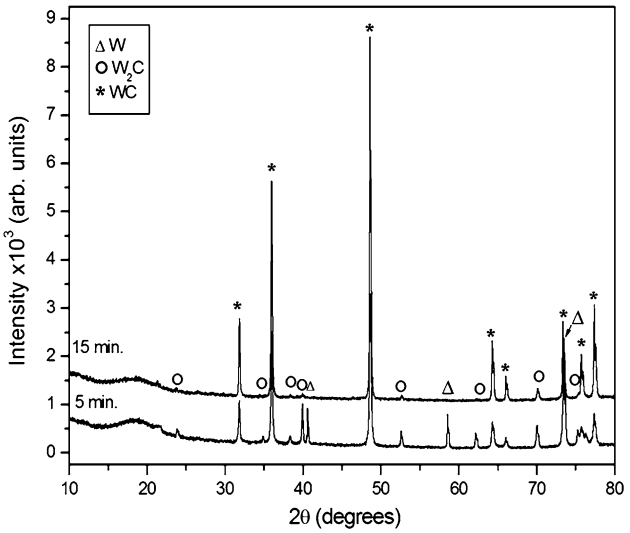

Fig. 3 XRD spectra of the filament–surface operated at 1400 °C for 5 and 15 min

W phases. The appearance of the WC phase is more rapid than previously reported for diamond synthesis [15], and is attributed to the higher CH_4 concentration and deposition pressure used.

Operating the W-filament at 1600 °C for 5 min results in the deposition of hemispherical deposits, of diameter ~35 μm, which are carbonaceous according to EDS analysis performed at 12 kV (see Fig. 4a and b). The formation of these carbon deposits, referred to as carbon microspheres, has been reported recently [22] and its growth mechanism involves the adsorption of hydrocarbon species onto the filament surface followed by the formation of tungsten-carbide microspheres which act as nucleation centres for the growth of carbon microspheres. XRD analysis (Fig. 4c) confirms, from the emergence of the diffraction peak at 2θ–26°, that the microspheres are graphitic. The graphitic microspheres eventually become more densely packed as the exposure time increases and appear to be growing preferentially along the grooves of the filament, ultimately resulting in an encapsulating layer after 60 min of exposure, as shown in Fig. 4d.

The temperature dependence of the carburization process becomes more apparent when increasing the temperature to 1800 °C. Figure 5 reveals that cracks form along the length of the filament after 5 min and that the graphitic microspheres only appear on the surface after 15 min. The filament crystals re-aligned themselves perpendicular to the filament-axis during carburization, as illustrated in the inset of Fig. 5a. This is indicative of a diffusion-based growth, which is characteristic for carburization [1].

Figure 6a shows that the graphitic microspheres initially grow inside the cracks of the filament after 15 min when increasing the temperature to 2000 °C. Prolonged exposure of the filament for 60 min again results in the encapsulation of the filament with a thicker solid graphitic layer as compared to 1600 °C, as shown in Fig. 6b. Cross sections of the carburized W-filament operated at 2000 °C for 15 and 60 min were prepared in order to observe the transformation of its internal structure (see Fig. 6c, d). After 15 minutes, the central core of the filament corresponds to pure W, whereas the surface displays cracks, which are the indicative of a carbide region as deduced from the XRD analysis. After 60 min of carburization, the filament diameter increases to approximately 600 μm and is covered by a solid graphite layer, approximately 180 μm thick, that is composed of sheets. Moreover, the cracks extend through the entire filament, indicating a fully carburized filament [1, 15].

The distinguishable feature of HFCVD over its thermal counterpart is its inherent characteristic to generate copious concentrations of atomic hydrogen through the catalytic dissociation of H_2 into atomic hydrogen by the heated W-filaments [23, 24]. This characteristic is especially

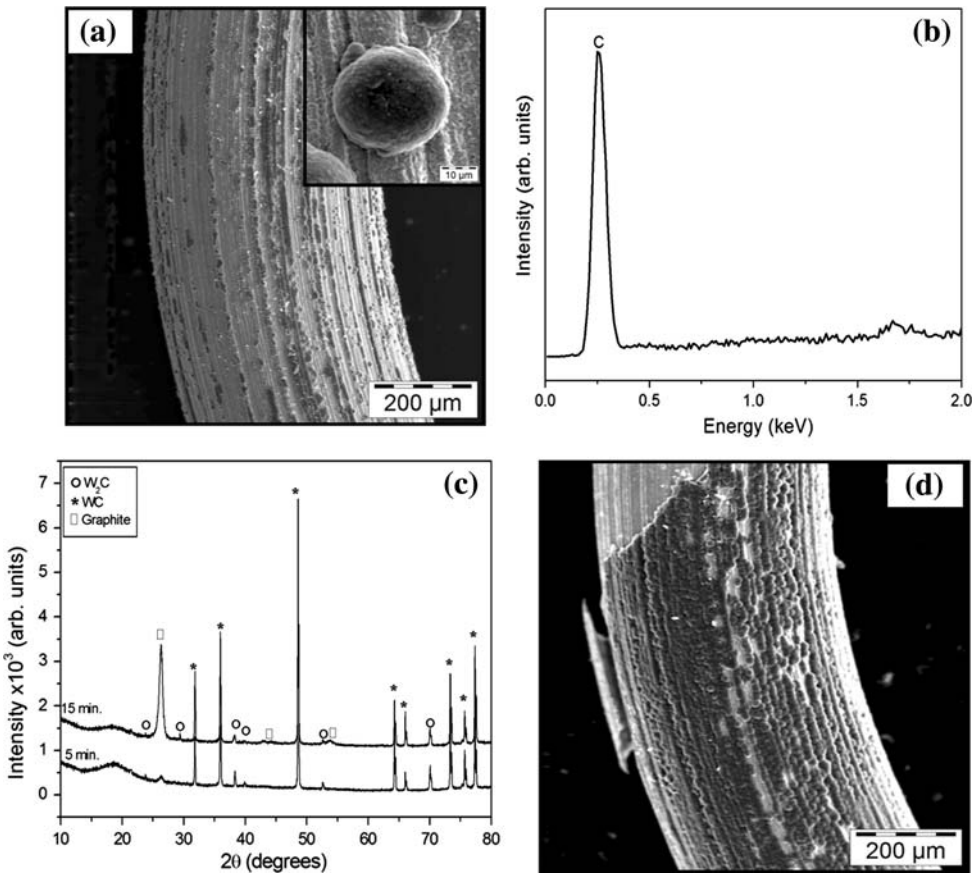

Fig. 4 **a** Secondary electron SEM micrograph of the filament–surface operated at 1600 °C for 5 min, **b** EDS spectrum of the globule shown in the inset of (**a**), **c** XRD spectra of the filament–surface operated at 1600 °C for 5 min, **d** secondary electron SEM micrograph of the filament–surface operated at 1600 °C for 60 min

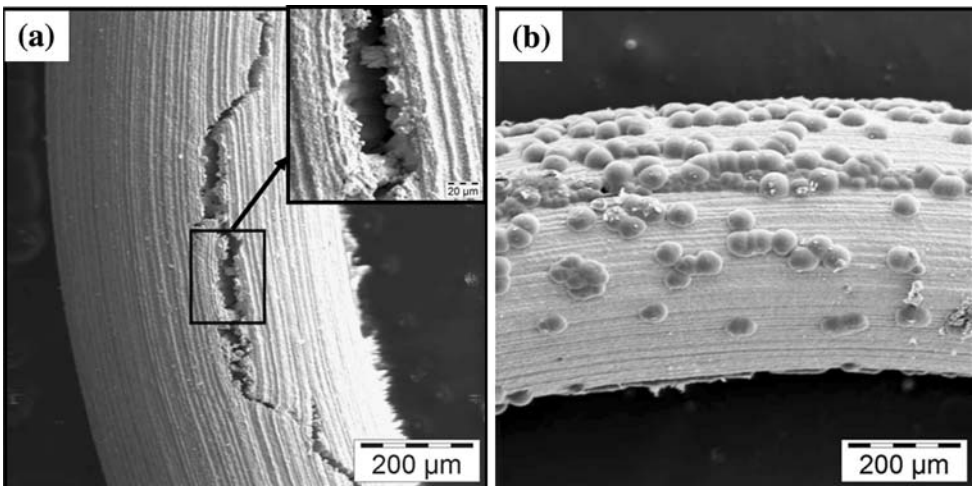

Fig. 5 Secondary electron SEM micrographs of the filament–surface operated at 1800 °C for **a** 5 min and **b** 15 min. The inset of (**a**) is at a higher magnification

beneficial to the deposition of CNTs, since atomic hydrogen etches amorphous carbon bonds and prevents the deposition of encapsulating carbon layers on the catalysts particles, thereby maintaining their activity [25]. However, the formation of solid graphitic layers on the filament–surface has shown to inhibit the catalytic ability of the filament to produce atomic hydrogen and has been consequently referred to as filament poisoning [23]. The results presented in this study therefore suggest that operating W-filaments at temperatures above 1600 °C is not desirable as filament poisoning occurs within the first 5 min of deposition, which is detrimental to the growth of CNTs with high purity.

The structural changes of the filament are clearly demonstrated by its effect on the temperature, as illustrated in Fig. 7, where the evolution of the filament temperature is plotted as a function of time for the initial temperatures of 1400 and 2000 °C. The increase in the filament temperature during the first 5 min is attributed to the appearance of

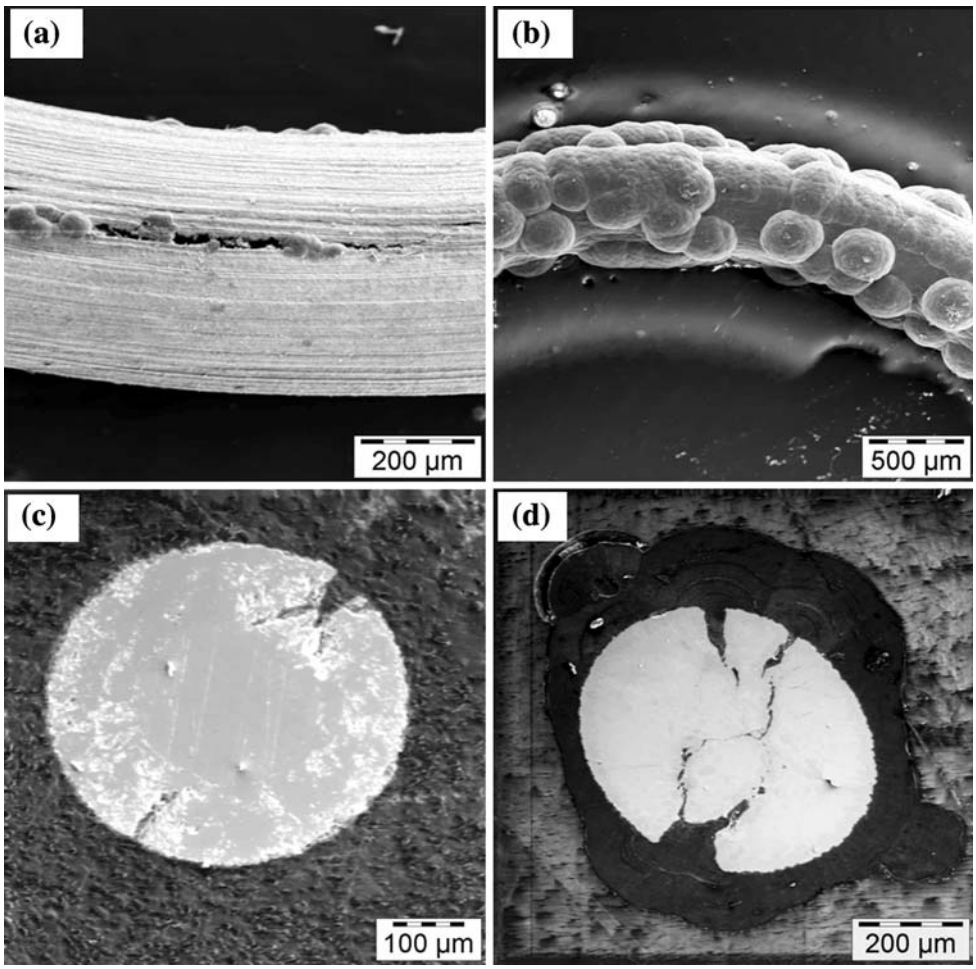

Fig. 6 Secondary electron SEM micrographs of the filament–surface operated at 2000 °C for **a** 15 min and **b** 60 min and of the cross sections of the filament operated at 2000 °C for **c** 15 min and **d** 60 min

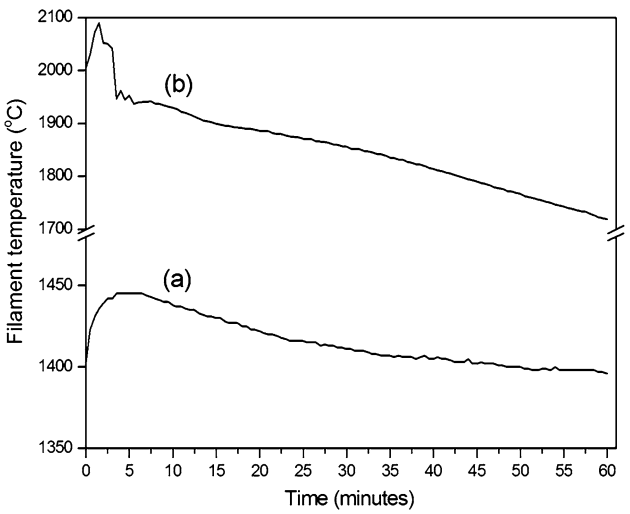

Fig. 7 Filament temperature as a function of exposure time for initial temperatures of (a) 1400 °C and (b) 2000 °C

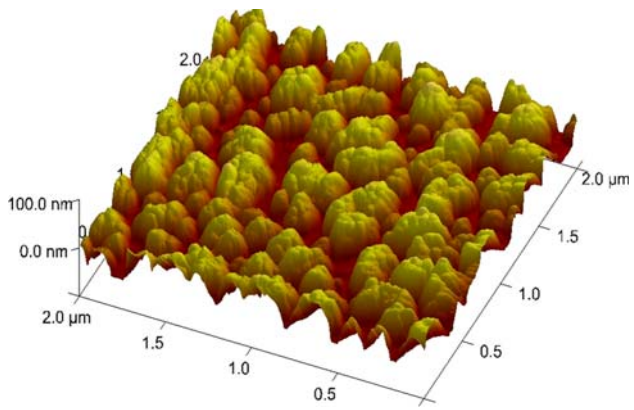

Fig. 8 AFM topograph of the $Ni/SiO_2/Si$ substrate after annealing

the W_2C and WC phases, which have higher resistivities than W. At 1400 °C, the temperature gradually starts to decrease after 5-min exposure to its initial value after 60 min. This is due to the enhancement of the WC phase, which has a lower resistivity than W_2C. In contrast, at 2000 °C the graphite layer becomes thicker with increased exposure times, resulting in an increased filament diameter. This observation, in conjunction with the higher emissivity of graphite ($\sim$0.9), results in a rapid decrease in the temperature to a final value of $\sim$1700 °C after 60 min.

So far, this contribution suggests 1400 °C as the optimum filament temperature for the deposition of CNTs at

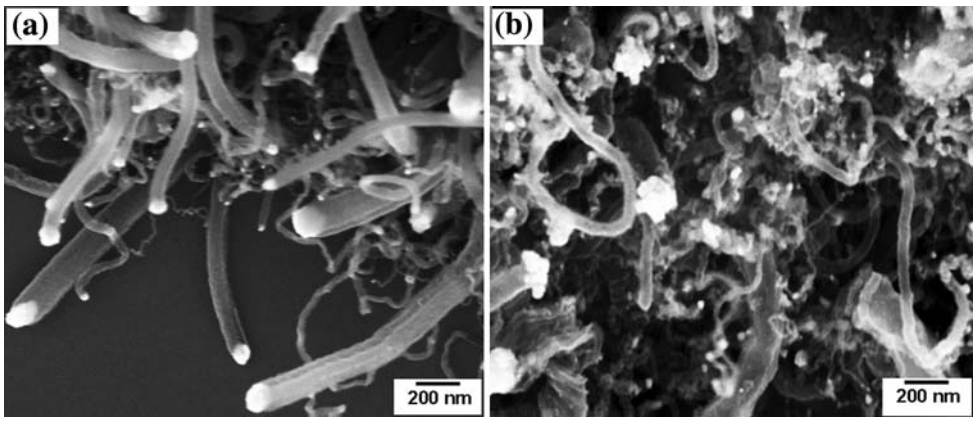

Fig. 9 Secondary electron SEM micrographs of MWCNTs deposited at a filament temperature of **a** 1400 °C and **b** 1600 °C

the deposition conditions described. As a preliminary comparative investigation, CNTs were synthesized on a $Ni/SiO_2/Si$ substrate at a filament temperature of 1400 and 1600 °C for a deposition time of 15 min, where the required nano-sized Ni-islands were prepared by annealing the substrate at 500 °C for 20 min in a 100 sccm H_2 flow at a pressure of 30 mTorr. It has been reported that no external catalyst for the CNT synthesis by HFCVD is required, since the W filament provides the catalyst necessary for CNT growth [26]. However, in this study the catalyst was prepared externally to enable more control over the catalyst morphology, as described above. Figure 8 shows an atomic force microscopy (AFM) topograph of the substrate after annealing, which confirms the formation of Ni islands of diameters ranging from 50 to 200 nm. The SEM micrographs, depicted in Fig. 9, demonstrate that straight multi-walled CNTs (MWCNTs) with minimal defects and a low degree of buckling are observed for a filament temperature of 1400 °C. The MWCNTs deposited at 1600 °C are more entangled with a high degree of surface coverage by amorphous carbon. The increased defect density at 1600 °C is attributed to the decrease in the concentration of atomic hydrogen during deposition, caused by the onset of filament poisoning by the formation of the graphitic microspheres on the W-filament.

Conclusion

The results demonstrate that the structure, morphology and temperature of the W-filament are not stable during typical CNT deposition conditions. SEM and XRD reveal that both WC and W_2C phases nucleate on the surface of the filament after 5 min at temperatures $\geq$1400 °C. At temperatures $\geq$1600 °C, graphitic microspheres and cracks form along the length of the filament after 5 min. The microspheres eventually grow in size and density to eventually encapsulate the filament after 60 min, which inhibits the filament's ability to produce atomic hydrogen that result in defect-rich CNTs. Furthermore, in situ temperature measurements reveal that the encapsulation process induces a temperature drop of $\sim$300 °C.

Acknowledgements The authors acknowledge the financial support of the Department of Science and Technology, the National Research Foundation and the Council for Scientific and Industrial Research (Project No. HGERA2S) of South Africa. The authors are especially thankful to Mr. Adrian Josephs (Microscopy Unit, University of the Western Cape) for his assistance with the SEM measurements and sample preparation.

References

1. Moustakas TD (1989) Solid State Ionics 32–33:861
2. Park SS, Lee JY (1993) J Mater Sci 28:1799. doi:10.1007/BF00595748
3. Sein H, Ahmed W, Hassan U, Ali N, Cracio JJ, Jackson MJ (2002) J Mater Sci 37:5057. doi:10.1023/A:1021043817134
4. Fortunato W, Chiquito AJ, Galzerani JC, Moro JR (2007) J Mater Sci 42:7331. doi:10.1007/s10853-007-1575-0
5. Rastogi AC, Desu SB (2005) Polymer 46:3440
6. Filonovich SA, Ribeiro M, Rolo AG, Alpuim P (2008) Thin Solid Films 516:576
7. Weissenbacher R, Haubner R, Aigner K, Lux B (2002) Diamond Relat Mater 11:191
8. Pal S, Jacob C (2006) J Mater Sci 41:5429. doi:10.1007/s10853-006-0270-x
9. Dillon AC, Mahan AH, Alleman JL, Heben MJ, Parilla PA, Jones KM (2003) Thin Solid Films 430:292
10. Sommer M, Smith FW (1990) J Mater Res 511:2433
11. Van der Werf CHM, Van Veenendaal PATT, Van Veen MK, Hardeman AJ, Rusche MYS, Rath JK, Schropp REI (2003) Thin Solid Films 430:46
12. Roger J, Audubert F, Petitcorps YL (2008) J Mater Sci 43:3938. doi:10.1007/s10853-007-2334-y
13. Kromka A, Janík J, Šatka A, Pavlov J, Červeň I (2001) Acta Physica Slovaca 51:359
14. Sommer M, Mui K, Smith FW (1989) Solid State Commun 69:775
15. Schwarz S, Zeiler E, Rosiwal SM, Singer RF (2002) Mater Sci Eng A 335:236
16. Okoli S, Haubner R, Lux B (1991) Surf Coat Technol 47:585
17. Matsubara H, Sakuma T (1990) J Mater Sci 25:4472. doi:10.1007/BF00581110

18. Davidson CF, Alexander GB, Wadsworth ME (1979) Metall Trans A 10A:1059
19. Wolden C, Gleason KK (1994) J Appl Phys 62:3102
20. Arendse CJ, Malgas GF, Scriba MR, Cummings FR, Knoesen D (2007) J Nanosci Nanotechnol 7:3638
21. International Centre for Diffraction Data (ICDD): W (89-3012), W_2C (79-0743), WC (89-2727) and graphite (75-1621)
22. Vieira SMC, Rego CA, Birkett PR (2008) Diamond Relat Mater 17:100
23. Hernberg R, Li DM, Mäntylä T (1998) Diamond Relat Mater 7:1709
24. Langmuir L (1912) J Am Chem Soc 34:1310
25. Honda S, Katayama M, Lee K, Ikuno T, Ohkura S, Oura K, Furuta H, Hirao T (2003) Jpn J Appl Phys 42:L441
26. Seo HK, Ansari SG, Kim GS, Kim YS, Shin HS (2004) J Mater Sci 39:5771. doi:10.1023/B:JMSC.0000040088.09431.e6